Supplemental Document

OPTICA QUANTUM

Squeezing-enhanced quantum sensing with quadratic optomechanics: supplement

Sheng-Dian Zhang,[1,†] Jie Wang,[1,†] Qian Zhang,[1,†] Ya-Feng Jiao,[1] Yun-Lan Zuo,[1] Şahin K. Özdemir,[2] Cheng-Wei Qiu,[3] Franco Nori,[4,5] and Hui Jing[1,*]

[1] *Key Laboratory of Low-Dimensional Quantum Structures and Quantum Control of Ministry of Education, Department of Physics and Synergetic Innovation Center for Quantum Effects and Applications, Hunan Normal University, Changsha 410081, China*
[2] *Department of Engineering Science and Mechanics, and Materials Research Institute, Pennsylvania State University, University Park, State College, Pennsylvania 16802, USA*
[3] *Department of Electrical and Computer Engineering, National University of Singapore, Singapore 117583, Singapore*
[4] *Theoretical Quantum Physics Laboratory, RIKEN Cluster for Pioneering Research, Wako-shi, Saitama 351-0198, Japan*
[5] *Physics Department, The University of Michigan, Ann Arbor, Michigan 48109-1040, USA*
[†] *The authors contributed equally to this work*
[*] *jinghui73@foxmail.com*

Supplement DOI: https://doi.org/10.6084/m9.figshare.26031511

Parent Article DOI: https://doi.org/10.1364/OPTICAQ.523480

Supplemental Material for "Squeezing-Enhanced Quantum Sensing with Quadratic Optomechanics"

Sheng-Dian Zhang,[1,*] Jie Wang,[1,*] Qian Zhang,[1,*] Ya-Feng Jiao,[1] Yun-Lan Zuo,[1]
Şahin K. Özdemir,[2] Cheng-Wei Qiu,[3] Franco Nori[4,5] and Hui Jing[1,†]

[1] *Key Laboratory of Low-Dimensional Quantum Structures and Quantum Control of Ministry of Education, Department of Physics and Synergetic Innovation Center for Quantum Effects and Applications, Hunan Normal University, Changsha 410081, China*
[2] *Department of Engineering Science and Mechanics, and Materials Research Institute, Pennsylvania State University, University Park, State College, Pennsylvania 16802, USA*
[3] *Department of Electrical and Computer Engineering, National University of Singapore, Singapore 117583, Singapore*
[4] *Theoretical Quantum Physics Laboratory, RIKEN Cluster for Pioneering Research, Wako-shi, Saitama 351-0198, Japan*
[5] *Physics Department, The University of Michigan, Ann Arbor, Michigan 48109-1040, USA*
[*] *These authors contribute equally to this work*
[†] *To whom correspondence should be addressed; E-mail: jinghui73@foxmail.com*

(Dated: June 13, 2024)

Here, we present more technical details on quantum-squeezing-enhanced quadratic optomechanical sensing, including: (1) detailed derivations of the linearized Hamiltonian; (2) degenerate optical parametric oscillations; (3) discussions on stability conditions; (4) noise spectrum and mechanical response characterizations; (5) signal-to-noise ratio and the optimal variance of the rotated field quadrature; (6) main classical hurdles to quantum-noise-limited measurements; (7) the effect of the fluctuations of the pump mode; (8) extended applications to the state-of-the-art quantum sensors.

S1. DERIVATION OF THE LINEARIZED HAMILTONIAN

In our cavity optomechanical (COM) system, the pump laser with frequency ω_p has twice the frequency of the signal laser (ω_s). Each laser tone (pump and signal) is quasi-resonant with a particular optical normal mode of the a Fabry-Pérot cavity, thus we refer to these optical modes as pump and signal mode, respectively [S1]. The flexible dielectric membrane is placed at a location of $q_0 = j\lambda_p/4 = k\lambda_s/4$ (j, k integers) [S2], i.e., the common node (or antinode) of the intracavity standing waves [S3], where λ_p and λ_s are the resonant wavelengths for the pump and signal modes, respectively. We then form a realistic description incorporating intrinsic losses and the coupling of the mechanical resonator to the optical modes, which yields the total Hamiltonian in a rotating frame [S4, S5]:

$$\begin{aligned}\hat{H} =& \hbar\Delta_c\hat{a}^\dagger\hat{a} + \hbar\Delta_p\hat{a}_p^\dagger\hat{a}_p + \frac{\hbar}{2}\Omega_m\left(\hat{q}_m^2+\hat{p}_m^2\right) - \hbar\hat{q}_m^2\left(g_0\hat{a}^\dagger\hat{a} + g_p\hat{a}_p^\dagger\hat{a}_p\right)\\ &+ \mathrm{i}\hbar\chi^{(2)}\left(\hat{a}^{\dagger 2}\hat{a}_p\mathrm{e}^{\mathrm{i}\theta} - \hat{a}^2\hat{a}_p^\dagger\mathrm{e}^{-\mathrm{i}\theta}\right) + \mathrm{i}\hbar\left(\mathcal{E}_c\hat{a}^\dagger + \mathcal{E}_p\hat{a}_p^\dagger - \mathrm{H.C.}\right),\end{aligned} \tag{S1}$$

where we wrote in a frame where the pump and signal modes phase space rotate at frequency ω_p and ω_s, respectively, and the driving amplitudes are $|\mathcal{E}_c| = \sqrt{\kappa\eta_c P_c/(\hbar\omega_s)}$, $|\mathcal{E}_p| = \sqrt{\kappa_p\eta_p P_p/(\hbar\omega_p)}$. The detunings of the optical modes are $\Delta_c = \Omega_c - \omega_s$, $\Delta_p = \Omega_p - \omega_p$, with g_0 and g_p the COM coupling strength of the signal and pump modes, respectively.

Thus, the equations of motion can be given by

$$\begin{aligned}\dot{\hat{a}} &= -\left(i\Delta_c + \frac{\kappa}{2}\right)\hat{a} + ig_0\hat{a}\hat{q}_m^2 + 2\chi^{(2)}\hat{a}^\dagger\hat{a}_p e^{i\theta} + \mathcal{E}_c,\\ \dot{\hat{a}}_p &= -\left(i\Delta_p + \frac{\kappa_p}{2}\right)\hat{a}_p + ig_p\hat{a}_p\hat{q}_m^2 - \chi^{(2)}\hat{a}^2 e^{-i\theta} + \mathcal{E}_p,\\ \dot{\hat{q}}_m &= \Omega_m\hat{p}_m,\\ \dot{\hat{p}}_m &= -\Omega_m\hat{q}_m - \Gamma_m\hat{p}_m + 2\hat{q}_m\left(g_0\hat{a}^\dagger\hat{a} + g_p\hat{a}_p^\dagger\hat{a}_p\right).\end{aligned} \tag{S2}$$

To proceed, we derive the classical equations for the steady-state values under the condition of strong optical driving

$$\begin{aligned}-\left(i\Delta + \frac{\kappa}{2}\right)\alpha + 2\chi^{(2)}e^{i\theta}\alpha\alpha_p + |\mathcal{E}_c|\,e^{i\Phi} &= 0,\\ -\left(i\Delta' + \frac{\kappa+p}{2}\right)\alpha_p - \chi^{(2)}e^{-i\theta}\alpha^2 + |\mathcal{E}_p|\,e^{i\varphi} &= 0,\\ -\Omega_m + 2g_0\alpha^*\alpha + 2g_p\alpha_p^*\alpha_p &= 0,\end{aligned} \tag{S3}$$

where Φ (φ) is the phase of the pump (signal) laser. Herein, we choose $\frac{\kappa}{2} = \frac{\kappa_p}{2} = \frac{\kappa}{2}$, $g_0 = g_0 = \frac{g_p}{4}$, then the steady-state solutions are

$$\begin{aligned}
2g_0\alpha_c^*\alpha_c &= \Omega_m - 2g_p\alpha_p^*\alpha_p, \\
\alpha_c^*\alpha_c &= \frac{\Omega_m - 2g_p\alpha_p^*\alpha_p}{2g_0} = \frac{\Omega_m - 8g_0\alpha_p^*\alpha_p}{2g_0} = \frac{\Omega_m}{2g_0} - 4\alpha_p^*\alpha_p, \\
&\quad -\left(i\Delta + \frac{\kappa}{2}\right)\alpha_c + 2\chi^{(2)}e^{i\theta}\alpha_c\alpha_p + |\mathcal{E}_c|\,e^{i\Phi} = 0, \\
&-\left(i\Delta' + \frac{\kappa}{2}\right)\alpha_p - \chi^{(2)}e^{-i\theta}\left(\frac{\Omega_m}{2g_0} - 4\,|\alpha_p|^2\right) + |\mathcal{E}_p|\,e^{i\Psi} = 0 \\
&\quad -\sqrt{\Delta'^2 + \frac{\kappa^2}{4}}\alpha_p - \chi^{(2)}\left(\frac{\Omega_m}{2g_0} - 4\alpha_p^2\right) + |\mathcal{E}_p| = 0, \\
&\quad 4\chi^{(2)}\alpha_p^2 - \sqrt{\Delta'^2 + \frac{\kappa^2}{4}}\alpha_p + |\mathcal{E}_p| - \frac{\chi^{(2)}\Omega_m}{2g_0} = 0.
\end{aligned} \tag{S4}$$

Thus,

$$\begin{aligned}
\alpha_p &= \frac{\sqrt{\Delta'^2 + \frac{\kappa^2}{4}} - \sqrt{\Delta'^2 + \frac{\kappa^2}{4} - 16\chi^{(2)}\left(|\mathcal{E}_p| - \frac{\chi^{(2)}\Omega_m}{2g_0}\right)}}{8\chi^{(2)}}, \\
&= \frac{\sqrt{\Delta'^2 + \frac{\kappa^2}{4}}}{8\chi^{(2)}} - \frac{\sqrt{\Delta'^2 + \frac{\kappa^2}{4} - 16\chi^{(2)}\left(|\mathcal{E}_p| - \frac{\chi^{(2)}\Omega_m}{2g_0}\right)}}{8\chi^{(2)}}, \\
&= \frac{1}{8\chi^{(2)}}\sqrt{\frac{\kappa^2 + 4\Delta'^2}{4}} - \frac{1}{8\chi^{(2)}}\sqrt{\frac{\kappa^2 + 4\Delta'^2}{4} - 16\chi^{(2)}\left(|\mathcal{E}_p| - \frac{\chi^{(2)}\Omega_m}{2g_0}\right)}, \\
&= \frac{1}{16\chi^{(2)}}\sqrt{\kappa^2 + 4\Delta'^2} - \sqrt{\frac{\kappa^2 + 4\Delta'^2}{4\times 64\chi^{(2)2}} - \frac{16\chi^{(2)}}{64\chi^{(2)2}}\left(|\mathcal{E}_p| - \frac{\chi^{(2)}\Omega_m}{2g_0}\right)}, \\
&= \frac{1}{16\chi^{(2)}}\sqrt{\kappa^2 + 4\Delta'^2} - \sqrt{\frac{\kappa^2 + 4\Delta'^2}{16\times 16\chi^{(2)2}} - \frac{1}{4\chi^{(2)}}\left(|\mathcal{E}_p| - \frac{\chi^{(2)}\Omega_m}{2g_0}\right)}.
\end{aligned} \tag{S5}$$

The external force is described as $\hat{F}_{\rm in} = \hat{F}_{\rm th} + \hat{F}_{\rm sig}$, where $\hat{F}_{\rm th} = \hat{\mathcal{F}}_{\rm th}/\sqrt{2\hbar m_{\rm eff}\Gamma_m\Omega_m}$ and $\hat{F}_{\rm sig} = \hat{\mathcal{F}}_{\rm sig}/\sqrt{2\hbar m_{\rm eff}\Gamma_m\Omega_m}$ are the scaled thermal force and the detected force signal with dimension $\mathrm{Hz}^{1/2}$, respectively. The variables $\delta\hat{a}_{\rm in}$ and $\delta\hat{a}_0$ represent the fluctuations at the coupling port and the port modelling internal losses, respectively. The single-photon coupling rate is denoted by $g_0 = g_{\rm om}q_{\rm zp}^2$, and the quadratic coupling strength is written as $g_{\rm om} = 8\pi^2 c\sqrt{R/(1-R)}/\left(\lambda_s^2 L\right)$ [S2], which can reach $1.54\,\mathrm{THz/nm^2}$ in experiment [S6]. Here we define the dimensionless mechanical quadratures as $\hat{q}_m = \hat{q}/q_{\rm zp}$ and $\hat{p}_m = \hat{p}/p_{\rm zp}$, where $q_{\rm zp} = \sqrt{\hbar/(m_{\rm eff}\Omega_m)}$, $p_{\rm zp} = \sqrt{\hbar m_{\rm eff}\Omega_m}$ are the standard deviations of the zero-point motion and momentum, respectively. Besides, the signal mode is characterized by a total loss rate $\kappa = \kappa_0 + \kappa_{\rm ex}$ with the efficiency defines as $\eta_c = \kappa_{\rm ex}/(\kappa_0 + \kappa_{\rm ex})$ describing the contribution of the input coupling loss rate to the total cavity loss rate. We note that in a very recent experiment [S7], the second-order nonlinearity was demonstrated with a value of $\chi^{(2)}/2\pi = 80\,\mathrm{kHz}$. Thus, it is possible to generate a nonlinear gain coefficient where α_p denotes the amplitude of the pump mode.

For simplicity, we choose $\alpha_p \in \mathbb{R} > 0$ and take intracavity field as the phase reference, i.e., $\alpha \in \mathbb{R} > 0$ [S1]. The solutions of the steady-state values can thus be expressed as

$$\begin{aligned}
\cos\theta &= \frac{1}{4G}\left(\kappa - \left|\frac{2\mathcal{E}_c}{\sqrt{n_c}}\right|\cos\Phi\right), \\
\bar{q}_m^2 &= \frac{1}{g_0}\left(\Delta_c - \left|\frac{\mathcal{E}_c}{\sqrt{n_c}}\right|\sin\Phi - 2G\sin\theta\right),
\end{aligned} \tag{S6}$$

where $n_c = \Omega_m/(2g_0)$, and he parametric phase depends on the phase Φ of the signal laser. Then, the displacement of the oscillator is directly proportional to the input force signal:

$$\delta\hat{q}[\Omega] = \chi_{\rm eff}^{(2)}[\Omega]\delta\hat{\mathcal{F}}_{\rm sig}[\Omega], \tag{S7}$$

where $\chi_{\rm eff}^{(2)}[\Omega]$ denotes the effective mechanical susceptibility:

$$\chi_{\rm eff}^{(2)}[\Omega] = \frac{1}{m_{\rm eff}\Omega_m\left(\chi_m^{-1}+\Sigma\right)},$$
$$\Sigma[\Omega] = \frac{16g^2(\Omega-\Delta-2G\sin\theta)}{\kappa^2-16G^2+4(\Omega-\Delta)^2}. \tag{S8}$$

For the resonance case without intracavity squeezing, the additional term $\Sigma[\Omega]$ is negligible. The effective susceptibility can be written at the simplest level as

$$\chi_{\rm eff}^{(2)}[\Omega] = -\frac{1}{m_{\rm eff}(\Omega^2+{\rm i}\Omega\Gamma_m)}. \tag{S9}$$

Here, we consider the effect of the fluctuations of the pump mode. For a strong pump field, this mode can be eliminated adiabatically, which yields the shifts of the cavity linewidth, the COM coupling rate, and the mechanical resonance frequency:

$$\kappa_s^{\rm eff} = \kappa_s + \frac{16\nu^2 n_s}{\kappa_p+2{\rm i}\Delta'}, \quad \Omega_m^{\rm eff} = -\frac{16G_p^2\Delta'}{\kappa_p^2+4\Delta'^2}, \quad G_s^{\pm} = G_s \pm \frac{4\nu\alpha_s G_p {\rm e}^{\pm{\rm i}\theta}}{\kappa_p+2{\rm i}\Delta'}, \tag{S10}$$

where $\Delta=\Delta_c-g_s\bar{q}_m^2$, $\Delta'=\Delta_p-g_p\bar{q}_m^2$, $G_s=g_s\bar{q}_m\sqrt{2n_s}$, and $G_p=g_p\bar{q}_m\sqrt{2n_p}$. Thus, the optical losses are slightly modified by the pump mode due to the photon up-conversion [S1]. The additional COM coupling and the mechanical eigenfrequency indicate the contributions of the photon-phonon coupling for the pump mode [S1]. Then, the fluctuations of the pump mode can be neglected under a large detuning and a small second-order nonlinearity [S1].

S2. THE OUTPUT QUADRATURES

After introducing phenomenologically the various dissipation mechanisms and associated input noise, the Hamiltonian yields readily the quantum Langevin equations

$$\begin{aligned}
\dot{\hat{a}} &= -\left({\rm i}\Delta_c+\frac{\kappa}{2}\right)\hat{a}+{\rm i}g_0\hat{a}\hat{q}_m^2+2Ge^{{\rm i}\theta}\hat{a}^\dagger \\
&\quad +\mathcal{E}_c+\sqrt{\eta_c\kappa}\hat{f}_{a,{\rm in}}+\sqrt{(1-\eta_c)\kappa}\hat{f}_{a,0}\,, \\
\dot{\hat{q}}_m &= \Omega_m\hat{p}_m\,, \\
\dot{\hat{p}}_m &= -\Omega_m\hat{q}_m-\Gamma_m\hat{p}_m+2g_0\hat{q}_m\hat{a}^\dagger\hat{a}+\sqrt{2\Gamma_m}\hat{F}_{\rm in}\,,
\end{aligned} \tag{S11}$$

where $\hat{f}_{a,{\rm in}}$ and $\hat{f}_{a,0}$ are the noise operators associated with the input cavity mirror and internal losses, respectively. The noise forces acting on the mechanical membrane are

$$\hat{F}_{\rm in} = \hat{F}_{\rm th}+\hat{F}_{\rm sig}\,, \tag{S12}$$

where $\hat{F}_{\rm th}$ and $\hat{F}_{\rm sig}$ are the scaled thermal force and the force signal to be detected, respectively, with dimension ${\rm Hz}^{1/2}$, respectively. All noise operators have zero mean values

$$\langle\hat{f}_{a,{\rm in}}\rangle = \langle\hat{f}_{a,0}\rangle = \langle\hat{F}_{\rm th}\rangle = \langle\hat{F}_{\rm sig}\rangle = 0. \tag{S13}$$

Because of the nonlinear COM interaction, Eqs. (S11) do not form a closed set of operator equations. We proceed by considering the situation of a strong driving, and expand each operator as the sum of its classical mean value and a small quantum fluctuation, i.e. $\hat{a}=\alpha+\delta\hat{a}$, $\hat{q}_m=\bar{q}_m+\delta\hat{q}_m$, and $\hat{p}_m=\bar{p}_m+\delta\hat{p}_m$, with $\langle\delta\hat{a}\rangle=\langle\delta\hat{q}_m\rangle=\langle\delta\hat{p}_m\rangle=0$. This yields the classical mean value equations of motion

$$\begin{aligned}
\dot{\alpha} &= -\left({\rm i}\Delta+\frac{\kappa}{2}\right)|\alpha|+2Ge^{{\rm i}\theta}|\alpha|+|\varepsilon_c|\,e^{\Phi}, \\
\dot{\bar{p}}_m &= -\Omega_m\bar{q}_m-\Gamma_m\bar{p}_m+2g_0\bar{q}_m|\alpha|^2\,, \\
\dot{\bar{q}}_m &= \bar{p}_m,
\end{aligned} \tag{S14}$$

where the effective optical detuning is $\Delta = \Delta_c - g_0\bar{q}_m^2$ and Φ describes the phase of the driving field. Here we take intracavity field as the phase reference, i.e., $\alpha \in \mathbb{R} > 0$, in which case the steady-state mean values become: $|\alpha|^2 = \Omega_m/2g_0$, $\bar{p}_m = 0$, and

$$|\bar{q}_m|^2 = \frac{1}{g_0}\left(\Delta_c - \left|\frac{\mathcal{E}_c}{\alpha}\right|\sin\Phi - 2G\sin\theta\right). \tag{S15}$$

We now introduce the 'position' and 'momentum'-like operators of the optical field,

$$\begin{aligned}\hat{q} &= \frac{1}{\sqrt{2}}\left(\hat{a}^\dagger + \hat{a}\right),\\ \hat{p} &= \frac{\mathrm{i}}{\sqrt{2}}\left(\hat{a}^\dagger - \hat{a}\right),\end{aligned} \tag{S16}$$

and the associated optical noise operators

$$\begin{aligned}\hat{f}_{q,\mathrm{in}} = \frac{1}{\sqrt{2}}\left(\hat{f}_{a,\mathrm{in}}^\dagger + \hat{f}_{a,\mathrm{in}}\right), \hat{f}_{p,\mathrm{in}} = \frac{\mathrm{i}}{\sqrt{2}}\left(\hat{f}_{a,\mathrm{in}}^\dagger - \hat{f}_{a,\mathrm{in}}\right);\\ \hat{f}_{q,0} = \frac{1}{\sqrt{2}}\left(\hat{f}_{a,0}^\dagger + \hat{f}_{a,0}\right), \hat{f}_{p,0} = \frac{\mathrm{i}}{\sqrt{2}}\left(\hat{f}_{a,0}^\dagger - \hat{f}_{a,0}\right).\end{aligned} \tag{S17}$$

In the Fourier domain expressions for the output quadratures:

$$\begin{aligned}\hat{q}_{\mathrm{out}}[\Omega] &= (\kappa/2 - 2G\cos\theta - i\Omega)^{-1}\left[\sqrt{\eta_c\kappa}\left(\Delta_c - 2G\sin\theta - g_0\hat{q}_m^2\right)\hat{p} + (\eta_c\kappa - 1)\,\hat{f}_{q,\mathrm{in}} + \kappa\sqrt{(1-\eta_c)\eta_c}\hat{f}_{q,0}\right],\\ \hat{p}_{\mathrm{out}}[\Omega] &= (\kappa/2 + 2G\cos\theta - i\Omega)^{-1}\left[-\sqrt{\eta_c\kappa}\left(\Delta_c - 2G\sin\theta - g_0\hat{q}_m^2\right)\hat{q} + (\eta_c\kappa - 1)\,\hat{f}_{p,\mathrm{in}} + \kappa\sqrt{(1-\eta_c)\eta_c}\hat{f}_{p,0}\right].\end{aligned} \tag{S18}$$

The essential step in quantum sensing is to observe the output fluctuations of physical quantities to be measured in the Fourier domain, i.e.,

$$\begin{pmatrix}\delta\hat{q}_{\mathrm{out}}\\ \delta\hat{p}_{\mathrm{out}}\end{pmatrix} = \begin{pmatrix}\mathcal{A}_- & \mathcal{B}_- & \mathcal{C}_- & \mathcal{D}_- & \mathcal{N}_-\\ -\mathcal{B}_+ & \mathcal{A}_+ & -\mathcal{D}_+ & \mathcal{C}_+ & \mathcal{N}_+\end{pmatrix}\left(\hat{f}_{q,\mathrm{in}}\ \ \hat{f}_{p,\mathrm{in}}\ \ \hat{f}_{q,0}\ \ \hat{f}_{p,0}\ \ \hat{F}_{\mathrm{in}}\right)^{\mathrm{T}}. \tag{S19}$$

where

$$\begin{aligned}\mathcal{A}_\pm[\Omega] &= \rho\kappa(\kappa/2 \pm 2G\cos\theta - i\Omega)^{-1}\eta_c - 1,\\ \mathcal{B}_+[\Omega] &= \rho\kappa(\Delta - 2G\sin\theta - 4g^2\chi_{\mathrm{m}})(\kappa/2 - 2G\cos\theta - i\Omega)^{-1}(\kappa/2 + 2G\cos\theta - i\Omega)^{-1}\eta_c\\ \mathcal{B}_-[\Omega] &= \rho\kappa(\Delta + 2G\sin\theta)(\kappa/2 - 2G\cos\theta - i\Omega)^{-1}(\kappa/2 + 2G\cos\theta - i\Omega)^{-1}\eta_c,\\ \mathcal{C}_\pm[\Omega] &= \rho\kappa(\kappa/2 \pm 2G\cos\theta - i\Omega)^{-1}\sqrt{(1-\eta_c)\eta_c},\\ \mathcal{D}_+[\Omega] &= \rho\kappa(\Delta - 2G\sin\theta - 4g^2\chi_{\mathrm{m}})(\kappa/2 - 2G\cos\theta - i\Omega)^{-1}(\kappa/2 + 2G\cos\theta - i\Omega)^{-1}\sqrt{(1-\eta_c)\eta_c},\\ \mathcal{D}_-[\Omega] &= \rho\kappa(\Delta + 2G\sin\theta)(\kappa/2 - 2G\cos\theta - i\Omega)^{-1}(\kappa/2 + 2G\cos\theta - i\Omega)^{-1}\sqrt{(1-\eta_c)\eta_c},\\ \mathcal{N}_+[\Omega] &= 2g\rho(\kappa/2 + 2G\cos\theta - i\Omega)^{-1}\chi_{\mathrm{m}}\sqrt{2\kappa\eta_c\Gamma_{\mathrm{m}}},\\ \mathcal{N}_-[\Omega] &= 2g\rho(\Delta + 2G\sin\theta)(\kappa/2 + 2G\cos\theta - i\Omega)^{-1}(\kappa/2 - 2G\cos\theta - i\Omega)^{-1}\chi_{\mathrm{m}}\sqrt{2\kappa\eta_c\Gamma_{\mathrm{m}}}\\ \rho &= \left[1 + (\kappa/2 - 2G\cos\theta - i\Omega)^{-1}(\kappa/2 + 2G\cos\theta - i\Omega)^{-1}(\Delta + 2G\sin\theta)\left(\Delta - 2G\sin\theta - 4g^2\chi_{\mathrm{m}}\right)\right]^{-1},\end{aligned} \tag{S20}$$

and $\chi_m = -\Omega_m/\left(\Omega^2 + \mathrm{i}\Omega\Gamma_m\right)$ is the mechanical susceptibility of the system, which quantifies the response of the oscillator to external forces. For the case without intracavity squeezing ($G = 0$, $\theta = 0$), the above coefficients related to the quadratic

coupling are

$$\begin{aligned}
\mathcal{A}_{\pm}^{'}[\Omega] &= \rho\kappa(\kappa/2 - i\Omega)^{-1}\eta_c - 1, \\
\mathcal{B}_{+}^{'}[\Omega] &= \rho\kappa(\Delta - 4g^2\chi_{\mathrm{m}})(\kappa/2 - i\Omega)^{-2}\eta_c \\
\mathcal{B}_{-}^{'}[\Omega] &= \rho\kappa\Delta(\kappa/2 - i\Omega)^{-2}\eta_c, \\
\mathcal{C}_{\pm}^{'}[\Omega] &= \rho\kappa(\kappa/2 - i\Omega)^{-1}\sqrt{(1-\eta_c)\eta_c}, \\
\mathcal{D}_{+}^{'}[\Omega] &= \rho\kappa(\Delta - 4g^2\chi_{\mathrm{m}})(\kappa/2 - i\Omega)^{-2}\sqrt{(1-\eta_c)\eta_c}, \\
\mathcal{D}_{-}^{'}[\Omega] &= \rho\kappa\Delta(\kappa/2 - i\Omega)^{-2}\sqrt{(1-\eta_c)\eta_c}, \\
\mathcal{N}_{+}^{'}[\Omega] &= 2g\rho(\kappa/2 - i\Omega)^{-1}\chi_{\mathrm{m}}\sqrt{2\kappa\eta_c\Gamma_{\mathrm{m}}}, \\
\mathcal{N}_{-}^{'}[\Omega] &= 2g\rho\Delta(\kappa/2 - i\Omega)^{-2}\chi_{\mathrm{m}}\sqrt{2\kappa\eta_c\Gamma_{\mathrm{m}}} \\
\rho^{'} &= \left[1 + (\kappa/2 - i\Omega)^{-2}\Delta\left(\Delta - 4g^2\chi_{\mathrm{m}}\right)\right]^{-1}.
\end{aligned} \tag{S21}$$

S3. SECOND-ORDER NONLINEAR PROCESSES

In the case of strong optical drives, the nonlinear gain coefficient is derived from the steady-state equations:

$$G = \chi^{(2)}\left(\tau - \sqrt{\tau^2 + \frac{\Omega_m}{8g_0} - \frac{|\mathcal{E}_p|}{4\chi^{(2)}}}\right), \tag{S22}$$

where $\tau = \sqrt{\kappa^2 + 4\Delta_p^2}/\left(16\chi^{(2)}\right)$, $|\mathcal{E}_p| = \sqrt{\kappa\eta_c P_p/(\hbar\omega_p)}$, and P_p quantifies the pump power for the $\chi^{(2)}$ crystal. The nonlinear gain coefficient is enhanced with the increase of the power of the pump laser and the second-order nonlinearity [Fig. S1(a), left panel], following the characteristic optical parametric oscillation (OPO) power curves [S7]. However, the photons circulating in the cavity is reduced when increasing the detuning of the pump field, which results in the suppression of the nonlinear gain coefficient [Fig. S1(a), right panel]. Figure S1(b) schematically illustrates the $\chi^{(2)}$ nonlinear process, where the OPO model can be treated as two coupled cavities with spontaneous parametric down-conversion [S7]. The visible pump laser at frequency ω_p drives the $\chi^{(2)}$ crystal, producing a pair of infrared signal and idler lights at frequencies ω_s and ω_i, which satisfies the energy-matching condition $\omega_p = \omega_s + \omega_i$. For degenerate OPOs ($\omega_s = \omega_i = \omega_p/2$), a single parametric oscillation is realized at half the frequency of the pump laser. Whereas for non-degenerate cases ($\omega_s \neq \omega_i$), the OPO process is operated at two distinct resonances centered about the pump.

S4. STABILITY CONDITIONS

The stability or instability of the system is determined by the signs of the real parts of the eigenvalues of the dynamical evolution matrix $\mathbf{M}$. To find the eigenvalues λ, it is necessary to solve the characteristic equation $\det(\mathbf{M} - \lambda\mathbf{I}) = 0$, which is reduced to an algebraic equation of the 4th degree: $\lambda^4 + \mathrm{M}_3\lambda^3 + \mathrm{M}_2\lambda^2 + \mathrm{M}_1\lambda + \mathrm{M}_0 = 0$. Applying the Routh-Hurwtiz method, we obtain the necessary and sufficient conditions for the system stability:

$$\begin{aligned}
&0 < \mathrm{M}_3, \qquad 0 < \mathrm{M}_3\mathrm{M}_2 - \mathrm{M}_1, \\
&0 < \mathrm{M}_0, \qquad 0 < \mathrm{M}_3\mathrm{M}_2\mathrm{M}_1 - \left(\mathrm{M}_1^2 + \mathrm{M}_3^2\mathrm{M}_0\right).
\end{aligned} \tag{S23}$$

These conditions allow to determine whether all the roots in the characteristic equation have negative real parts. Thus, we can use them to justify the system stability without solving the characteristic equation itself. Herein, we focus on the resonance case ($\Delta \approx \Delta_c = 0$), thereby the first three inequalities in Eq. (S23) yield the first two stability conditions: $G/\kappa < 0.25$, $-\pi < \theta < 0$. To proceed, by exploiting the last inequality in Eq. (S23), we formulate the stability criterion functions Θ as

$$\Theta = \mathrm{M}_3\mathrm{M}_2\mathrm{M}_1 - \left(\mathrm{M}_1^2 + \mathrm{M}_3^2\mathrm{M}_0\right). \tag{S24}$$

Then, the signs of Θ provide the remaining stability requirements:

$$\mathrm{sgn}\left(\Theta\right) = \begin{cases} 1, & \text{implies stability,} \\ \text{otherwise,} & \text{implies instability.} \end{cases} \tag{S25}$$

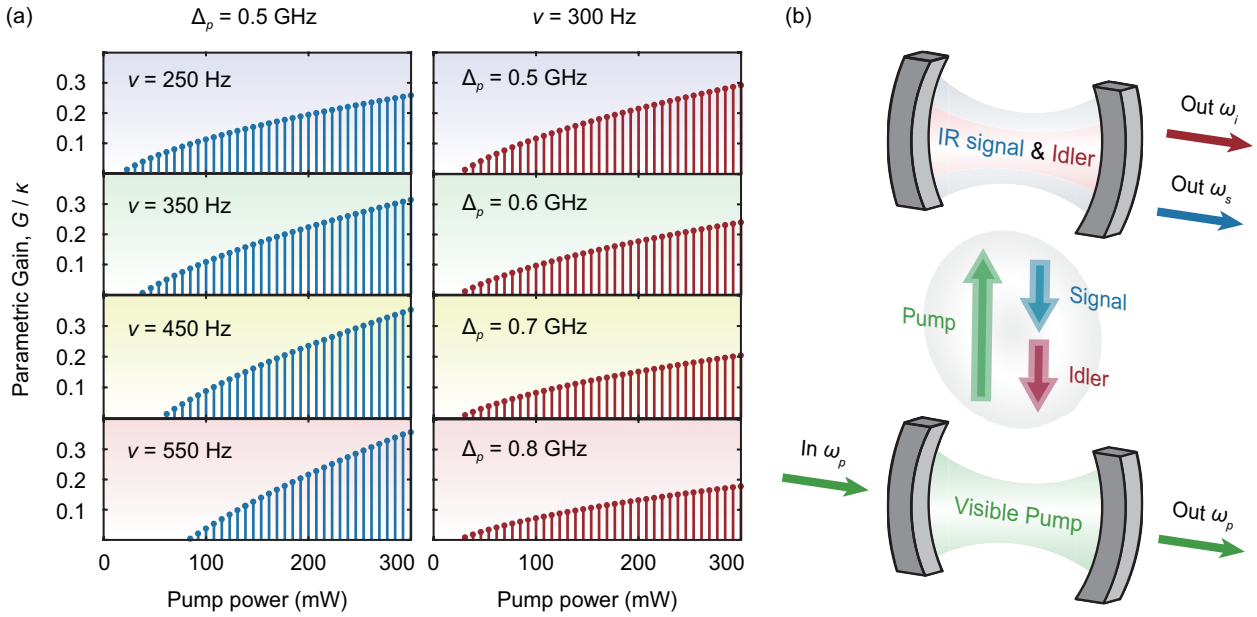

FIG. S1: Degenerate OPO process. (a) The parametric gain versus the pump power for the parametric oscillation process. The evolutions are shown at a red detuning of the pump field with $\Delta_p = 0.5\,\mathrm{GHz}$ (left panel) [S1] and a second-order nonlinearity of $\chi^{(2)} = 300\,\mathrm{Hz}$ (right panel) [S7]. The theoretical pump power threshold is tens of milliwatts, which is in agreement with the recent OPO experiment [S7]. (b) Schematic representation of the OPO model using two Fabry–Pérot cavities.

As shown in main text, the parameters used in our numerical calculations are chosen truly in the stable region. In particular, the required signal power can be derived from Eq. (S15):

$$P_c = \frac{\hbar\Omega_l n_c}{4\kappa\eta_c}\Big[(\kappa - 4G)^2 + 8G\kappa(1-\cos\theta)\Big], \tag{S26}$$

which is tens of microwatts and can be attained with accessible experimental conditions [S8]. In principle, a system tends to be sensitive to external perturbations in the unstable region. Then, the sensitive region in the stable realm locates near the dividing line between stability and instability.

S5. SIGNAL-TO-NOISE RATIO AND THE OPTIMAL VARIANCE

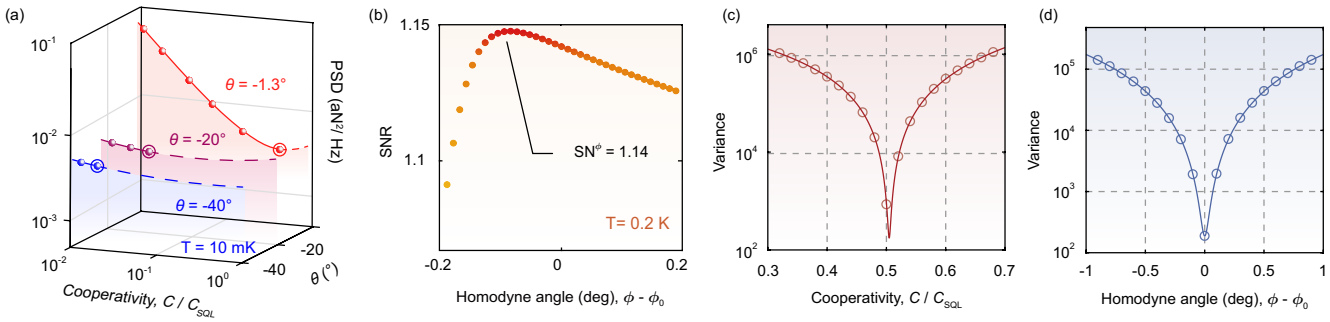

FIG. S2: Signal-to-noise ratio (snr) and the optimal variance. (a) Power spectral density (PSD) as a function of cooperativity and θ. The solid and dashed curves denote the PSD in the stable or unstable region, respectively, and the circles give the minimum PSD in the stable region. The bath temperature T =10 mK. (b) SNR for quadratic COM sensors. The reference phase is chosen as $\phi_0 = -98°$. The bath temperature T = 0.2 K. (c)-(d) The variance of the optimal quadrature. The multi-photon cooperativity is $C/C_{\mathrm{SQL}} = 0.5$, and the signal force spectrum is chosens $(0.1\,\mathrm{aN})^2/\mathrm{Hz}$ [S9].

The performance of the state-of-the-art sensors is commonly quantified by the signal-to-noise ratio (SNR). In our system, the spectral density and the SNR of the signal force are respectively estimated by [S10]

$$\bar{S}_{\mathrm{FF}}^{\mathrm{est},\phi}[\Omega]=\bar{S}_{\mathrm{FF}}^{\mathrm{sig}}+\bar{S}_{\mathrm{FF}}^{\phi},\qquad \mathrm{SN}^{\phi}[\Omega]=\frac{\bar{S}_{\mathrm{FF}}^{\mathrm{est},\phi}}{\bar{S}_{\mathrm{FF}}^{\mathrm{est},\phi}-\bar{S}_{\mathrm{FF}}^{\mathrm{sig}}}. \tag{S27}$$

The spectral density of the apparent force experienced by the oscillator is described as $\bar{S}_{\mathrm{FF}}^{\mathrm{est},\phi}$, and the spectral density of the signal force is described as $\bar{S}_{\mathrm{FF}}^{\mathrm{sig}}$. As shown in Fig. S2(a), the SNR can reach 1.14 at the temperature of 0.2 K.

Figure S2(b)-(c) characterizes the variance of the generalized rotated field quadrature, which is given by [S11]

$$V_{\mathrm{qq}}^{\phi}[\Omega]=\int_{-\infty}^{\infty}\mathrm{Re}\{\bar{S}_{\mathrm{qq}}^{\phi,\mathrm{out}}\}\frac{\mathrm{d}\Omega}{2\pi}, \tag{S28}$$

where the optical output spectrum is expressed as [S10]

$$\bar{S}_{\mathrm{qq}}^{\phi,\mathrm{out}}[\Omega]=\bar{S}_{\mathrm{qq}}^{\mathrm{out}}[\Omega]\cos^2\phi+\bar{S}_{\mathrm{pp}}^{\mathrm{out}}[\Omega]\sin^2\phi+\bar{S}_{\mathrm{pq}}^{\mathrm{out}}[\Omega]\sin(2\phi). \tag{S29}$$

Such a variance reaches its lowest value when choosing proper cooperativity and homodyne angle.

S6. EXTENDED APPLICATIONS TO PRECISION MEASUREMENTS

Table S1 provides a comparison of performance metrics for recently reported COM sensors including the force sensor described in this work.

Sensors	Experiment (Y/N)	Temperature	Mean phonon occupations	Reported sensitivity	Equivalent force sensitivity	References
Magnetometer	Y	300 K	1.1×10^{6}	$(400\ \mathrm{nT})^2\mathrm{Hz}$	$(2.4\ \mathrm{pN})^2\mathrm{Hz}$	[S12]
Magnetometer	Y	300 K	1.2×10^{6}	$(200\ \mathrm{pT})^2\mathrm{Hz}$	$(1.2\ \mathrm{fN})^2\mathrm{Hz}$	[S13]
Magnetometer	Y	300 K	$\sim1.0\times10^{6}$	$(5\ \mathrm{nT})^2\mathrm{Hz}$	$(0.75\ \mathrm{nN})^2\mathrm{Hz}$	[S14]
Torque sensor	Y	~1 mK	~2.8	$(1.3\ \mathrm{zN\,m})^2\mathrm{Hz}$	$(0.43\ \mathrm{fN})^2\mathrm{Hz}$	[S15]
Ultrasound sensor	Y	300 K	1.3×10^{8}	$(8\ \mu\mathrm{Pa})^2\mathrm{Hz}$	$\sim(370\ \mathrm{fN})^2\mathrm{Hz}$	[S16]
This work	N	300 K	6.2×10^{6}		$(10.2\ \mathrm{aN})^2\mathrm{Hz}$	
		10 K	2.1×10^{5}		$(1.86\ \mathrm{aN})^2\mathrm{Hz}$	
		0.2 K	4.2×10^{3}		$(0.26\ \mathrm{aN})^2\mathrm{Hz}$	

TABLE S1: Extended applications to the state-of-the-art COM sensors. The resolution of the accelerometers is quantified by noise-equivalent acceleration in units of $g^2\mathrm{Hz}$, where $1\,g=9.81\,\mathrm{m/s^2}$.

[S1] V. Peano, H. G. L. Schwefel, C. Marquardt, and F. Marquardt, "Intracavity Squeezing Can Enhance Quantum-Limited Optomechanical Position Detection through Deamplification," Phys. Rev. Lett. **115**, 243603 (2015).

[S2] M. Bhattacharya, H. Uys, and P. Meystre, "Optomechanical trapping and cooling of partially reflective mirrors," Phys. Rev. A **77**, 033819 (2008).

[S3] J. C. Sankey, C. Yang, B. M. Zwickl, A. M. Jayich, and J. G. E. Harris, "Strong and tunable nonlinear optomechanical coupling in a low-loss system," Nat. Phys. **6**, 707–712 (2010).

[S4] J.-Q. Liao and F. Nori, "Single-photon quadratic optomechanics," Sci. Rep. **4**, 6302 (2014).

[S5] W. Qin, A. Miranowicz, H. Jing, and F. Nori, "Generating Long-Lived Macroscopically Distinct Superposition States in Atomic Ensembles," Phys. Rev. Lett. **127**, 093602 (2021).

[S6] T. K. Paraïso, M. Kalaee, L. Zang, H. Pfeifer, F. Marquardt, and O. Painter, "Position-Squared Coupling in a Tunable Photonic Crystal Optomechanical Cavity," Phys. Rev. X **5**, 041024 (2015).

[S7] A. W. Bruch, X. Liu, J. B. Surya, C.-L. Zou, and H. X. Tang, "On-chip $\chi^{(2)}$ microring optical parametric oscillator," Optica **6**, 1361–1366 (2019).

[S8] X. Zhang, Q.-T. Cao, Z. Wang, Y.-x. Liu, C.-W. Qiu, L. Yang, Q. Gong, and Y.-F. Xiao, "Symmetry-breaking-induced nonlinear optics at a microcavity surface," Nat. Photonics **13**, 21–24 (2018).

[S9] David Hälg, Thomas Gisler, Yeghishe Tsaturyan, Letizia Catalini, Urs Grob, Marc-Dominik Krass, Martin Héritier, Hinrich Mattiat, Ann-Katrin Thamm, Romana Schirhagl, Eric C. Langman, Albert Schliesser, Christian L. Degen, and Alexander Eichler, "Membrane-based scanning force microscopy," Phys. Rev. Appl. **15**, L021001 (2021).

[S10] V. Sudhir, R. Schilling, S. A. Fedorov, H. Schutz, D. J. Wilson, and T. J. Kippenberg, "Quantum Correlations of Light from a Room-Temperature Mechanical Oscillator," Phys. Rev. X **7**, 031055 (2017).

[S11] C. Meng, G. A. Brawley, J. S. Bennett, M. R. Vanner, and W. P. Bowen, "Mechanical Squeezing via Fast Continuous Measurement," Phys. Rev. Lett. **125**, 043604 (2020).

[S12] S. Forstner, S. Prams, J. Knittel, E. D. Van Ooijen, J. D. Swaim, G. I. Harris, A. Szorkovszky, W. P Bowen, and H. Rubinsztein-Dunlop, "Cavity optomechanical magnetometer," Phys. Rev. Lett. **108**, 120801 (2012).

[S13] S. Forstner, E. Sheridan, J. Knittel, C. L. Humphreys, G. A. Brawley, H. Rubinsztein-Dunlop, and W. P. Bowen, "Ultrasensitive optomechanical magnetometry," Adv. Mater. **26**, 6348–6353 (2014).

[S14] B.-B. Li, J. Bílek, U. B. Hoff, L. S. Madsen, S. Forstner, V. Prakash, C. Schäfermeier, T. Gehring, W. P. Bowen, and U. L. Andersen, "Quantum enhanced optomechanical magnetometry," Optica **5**, 850–856 (2018).

[S15] M. Wu, A. C. Hryciw, C. Healey, D. P. Lake, H. Jayakumar, M. R. Freeman, J. P. Davis, and P. E. Barclay, "Dissipative and Dispersive Optomechanics in a Nanocavity Torque Sensor," Phys. Rev. X **4**, 021052 (2014).

[S16] S. Basiri-Esfahani, A. Armin, S. Forstner, and W. P. Bowen, "Precision ultrasound sensing on a chip," Nat. Commun. **10**, 132 (2019).